APPLIED PHYSICS LETTERS **89**, 233101 (2006)

Order enhancement and coarsening of self-organized silicon nanodot patterns induced by ion-beam sputtering

R. Gago[a]
Centro de Micro-Análisis de Materiales, Universidad Autónoma de Madrid, E-28049 Madrid, Spain

L. Vázquez
Instituto de Ciencia de Materiales de Madrid (CSIC), E-28049 Madrid, Spain

O. Plantevin[b] and T. H. Metzger
European Synchrotron Radiation Facility, F-38043 Grenoble Cedex, France

J. Muñoz-García and R. Cuerno
Departamento de Matemáticas and GISC, Universidad Carlos III de Madrid, E-28911 Leganés, Spain

M. Castro
Escuela Técnica Superior de Ingeniería, Universidad Pontificia de Comillas, E-28015 Madrid, Spain

(Received 19 July 2006; accepted 19 October 2006; published online 4 December 2006)

The temporal evolution of the characteristic wavelength (λ) and ordering range (ξ) of self-organized nanodot patterns induced during Ar^+ ion beam sputtering on Si(001) and Si(111) surfaces is studied by atomic force microscopy and grazing incidence x-ray diffraction. The patterns exhibit initial coarsening of λ (up to 54–60 nm) and increase in ξ (up to 400–500 nm) after which both features stabilize. The pattern formation is only weakly controlled by the crystallographic surface orientation, Si(111) surfaces showing a faster evolution into a proper stationary state. This trend is attributed to a higher sputtering rate at this orientation, as confirme by theoretical simulations.
© *2006 American Institute of Physics*. [DOI: 10.1063/1.2398916]

The current road to miniaturization demands for low-cost and large-scale compatible nanopatterning methods with reproducible and controllable features, achievement of high in-plane ordering being a crucial issue, e.g., for (opto)electronic devices.[1] Ion beam sputtering (IBS) is a promising technique since it induces self-organized regular patterns over large areas (several cm^2) onto metal, semiconductor, and insulator surfaces after a few minutes of irradiation.[2] In particular, ripple[3] and nanodot[4] morphologies can be produced onto amorphous materials or crystalline surfaces that amorphize upon ion bombardment. Theoretically, pattern formation by IBS can be understood as the interplay between the (unstable) dependence of the sputtering yield on surface curvature and stabilizing surface relaxation mechanisms such as surface diffusion.[5]

Complete understanding and control of the physical mechanisms involved in pattern formation by IBS is still lacking, issues such as crystallinity, in-plane correlation, and order remaining to be understood. Here, we study the time evolution of the quality of nanodot patterns induced by IBS onto the relevant Si(001) and Si(111) surfaces, in terms of in-plane order and correlation. Our results indicate that the pattern dynamics is qualitatively independent of the surface orientation, together with the occurrence of coarsening of the characteristic wavelength λ and simultaneous improvement of the short-range hexagonal order (as described by the correlation length ξ). Both features stabilize for long enough times, the Si(111) surface reaching earlier a proper stationary state as a result of its faster dynamics. We correlate this fact with the increased sputtering rate (SR) measured onto this orientation, which is confirme through comparison with theoretical models of IBS pattern formation.

Si(001) and Si(111) samples (p type, 0.3–1 Ω cm) were sputtered at normal incidence as described in Ref. 6. The SR was determined experimentally in all the processed samples by partially masking them during the sputtering process and measuring the resulting step edge height with a profilomete . It was observed that the SR was ~10% higher for Si(111) than for Si(001). The resulting surface topography was imaged by atomic force microscopy (AFM) with a Nanoscope IIIa equipment operating in tapping mode in air and using silicon cantilevers. The pattern characteristics were further analyzed by grazing incidence diffraction (GID) at the "Anomalous Scattering Beamline" (ID01) of the ESRF. The x-ray wavelength was 1.55 Å and the incidence angle was fixe at 0.2°, slightly below the critical angle for total external reflectio (0.22°). The exit angle was integrated on a position sensitive detector perpendicular to the sample surface. Measurements in reciprocal space were taken around in plane (220) and (2$\underline{2}$0) Bragg reflection for Si(001) and Si(111), respectively.

Figures 1(a)–1(d) show AFM images of Si(001) and Si(111) surfaces, respectively, sputtered at different times. The nanodot patterns are very similar for both surfaces, consisting in short-range hexagonal arrays of crystalline mounds of 40–60 nm width and 5–7 nm height (density of $\sim 3.5 \times 10^{10}$ cm^{-2}).[6] Both surfaces also display, superimposed onto the dot pattern, a smooth long-wavelength corrugation (~500 nm width and ~6 nm height) for $t > 20$ min, which clearly grows with time.

The evolution of λ is analyzed from the power spectral density (PSD) of the AFM images displayed in Fig. 2(a). These curves show a clear peak at $k = 1/\lambda$, related to the basic wavelength of the nanopattern. The peak position shifts to smaller wavenumbers (longer distances), evidencing

[a]Electronic mail: raul.gago@uam.es
[b]Present address: Centre de Spectrométrie Nucléaire et de Spectrométrie de Masse CNRS/IN2P3, Université Paris-Sud, UMR 8609, Orsay Campus F-91405, France.

 © 2006 American Institute of Physics

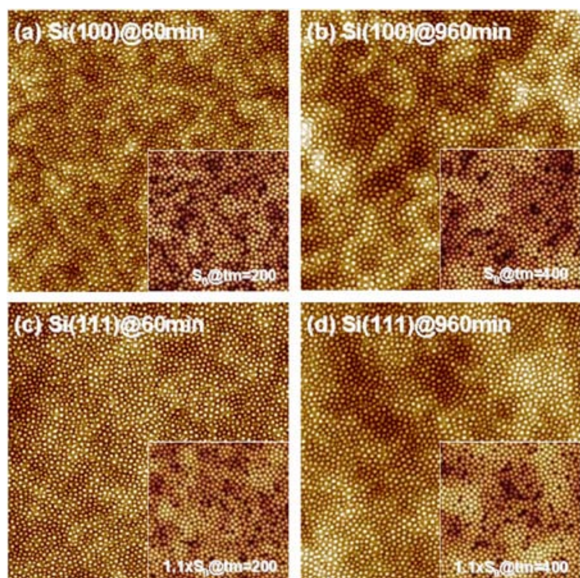

FIG. 1. (Color online) AFM 3×3 μm^2 images of Si(001) and Si(111) surfaces sputtered with 1.2 keV Ar$^+$ for different times (see labels). Insets: 2D views (length scales in arbitrary units) from numerical integration of Eq. (1) for different simulation times (tm) and surfaces with low (ν=0.68, κ=1, λ_1=0.028, and λ_2=0.136) and high (ν=0.748, κ=1, λ_1=0.308, and λ_2=0.1496) SRs.

coarsening of λ with ion dose for both substrates. The full width at half maximum of the PSD peak can be used to estimate ξ.[7] The PSD peak sharpens (i.e., ξ increases) and develops harmonics for longer irradiation times, both trends indicating enhancement of order with ion dose. The development of the long-wavelength corrugation is consistent with the negative slope of the corresponding PSD curves for $k < 1/\lambda$. Note that after 8 h of sputtering the PSD of Si(111) shows a clear power-law behavior with k for the smallest k, while the corresponding PSD of Si(001) is k independent for this range of wave vectors. This means that the former orientation is already at a stationary state (all wavelengths are correlated) that has not yet been reached for Si(001), suggesting faster dynamics for Si(111).

Figure 2(b) shows the GID angular scans for Si(001) and Si(111) sputtered at increasing ion dose. The appearance of

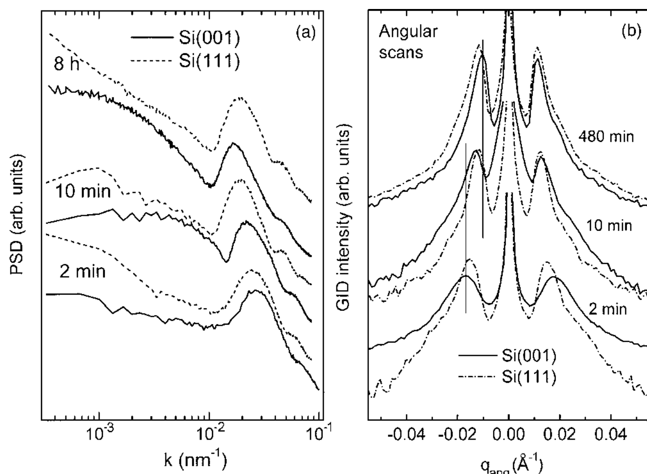

FIG. 2. (a) PSD from AFM images and (b) GID angular scans of Si(001) (solid lines) and Si(111) (dotted lines) sputtered for 2, 10, and 480 min. The spectra have been shifted vertically for clarity purposes and the GID intensity is shown in logarithmic scale. The vertical lines are "guides for the eyes" to show the peak shift.

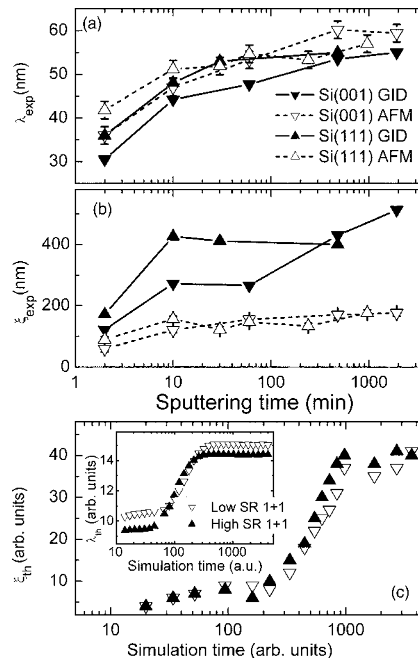

FIG. 3. Time evolution for the experimental (exp) values of (a) λ and (b) ξ during IBS of Si(001) and Si(111) surfaces derived from AFM and GID data. (c) Theoretical (th) evolution of ξ obtained from the 1+1 numerical integration of Eq. (1) using parameters as in Fig. 1 for high and low SR surfaces. Inset: evolution of λ_{th} for the same surfaces.

correlation peaks around the Bragg peak reveals the pattern formation and the crystalline character of the nanodot structures.[8] The peak position is related with λ and shifts towards smaller q values (larger distances) as the ion dose increases. Additionally, the correlation peak becomes more intense and sharpens with ion dose, indicating the enhancement of ordering. Both observations are consistent with the observed AFM trends. The quantificatio of λ and ξ by GID is done through a spectral fittin that considers the convolution of form and structure functions.[8]

Figures 3(a) and 3(b) compare the values of λ and ξ, respectively, obtained independently by AFM and GID. The AFM data are obtained by averaging over the results of up to three samples processed under the same conditions for each sputtering time (bars comprise statistic and sampling errors) whereas, due to limited access, synchrotron analysis was only performed on selected samples. AFM and GID data show a similar trend for λ, its values being quite consistent in the case of Si(111) while larger λ values are obtained by AFM than GID in the case of Si(001). Initially, λ coarsens with time until it saturates at ~54–60 nm for $t > 30$ min for both Si surfaces. In addition, ξ increases with ion dose before it saturates for large irradiation times. The saturated ξ values derived from AFM are very similar for both surfaces, being in the 150–170 nm range. However, the GID analysis yields ξ values two to three times larger than AFM. Also, within the temporal range studied here, ξ increases consistently with ion dose up to ~500 nm for Si(001), whereas in Si(111) a saturation value of ξ~400 nm is reached after 10–30 min of sputtering. Both AFM and GID data indicate that the pattern wavelength saturates earlier for Si(111) surfaces.

The present comparison shows that AFM and GID give similar qualitative trends for λ and ξ, but lead to different quantitative results. These differences can be understood from the different sampling statistics, since AFM has a rather local character while GID samples over larger areas. In any

case, these results show that the IBS pattern formation on both Si surfaces is quite similar, which supports the assumption that the nanopatterning process is mainly governed by the ion-induced thin amorphous surface layer, as already demonstrated onto GaSb.[9]

Regarding the pattern dynamics, the use of GID in our work allows for the quantitative analysis of λ and ξ with a higher resolution than in conventional AFM studies. The experimental results show a clear coarsening of λ with ion dose. This observation is relevant since, although coarsening has been reported in ripple formation,[10] the results for nanodot patterns on semiconductor surfaces are somehow controversial.[7,11–13] Moreover, our data evidence ordering enhancement with ion dose, as qualitatively pointed out previously for GaSb,[11] InP,[13] and Si[7] patterns by means of only AFM. It is important to note that, experimentally, the surface with lower SR shows a slower dynamics but can achieve asymptotically larger ordered domains [see Fig. 3(b)]. The dependence of the pattern formation dynamics on the SR and the temporal evolution of the pattern features reported here have been also observed by *in-situ* synchrotron studies on GaSb surfaces.[14]

The observed experimental pattern coarsening and ordering are incompatible with previous nonlinear extensions of Bradley and Harper (BH) seminal model,[5] which either neglect[15,16] or incorporate[17] redeposition in a phenomenological way. In contrast, a recently proposed hydrodynamic-type model[18] does account for both pattern coarsening and ordering by combining BH description of sputtering with the additional physical mechanisms of local redeposition and surface viscous flo . In this model, the equation describing the surface height $h(x,y,t)$ is given by[18]

$$\partial h/\partial t = -|\nu|\nabla^2 h - \kappa\nabla^4 h + \lambda_1(\nabla h)^2 - \lambda_2\nabla^2(\nabla h)^2, \qquad (1)$$

where, as in the BH model, the parameters in Eq. (1) are related with physical parameters of the sputtering and diffusion processes. In particular, all of them, except that related with surface diffusion (κ), are proportional to the SR.[18]

In order to understand the differences found experimentally between the two surface orientations, we have integrated Eq. (1) numerically considering that, under our experimental conditions, the SR was $\sim 10\%$ higher for Si(111) surfaces than for Si(001). Thus, as the model neglects target crystallinity, we have used this relative difference in SR to simulate the IBS pattern evolution in two model systems. Insets of Figs. 1(a) and 1(b) display the two-dimensional (2D) top-view images from the simulations for surfaces with a given $\mathrm{SR}=\mathrm{SR}_{001}=S_0$ [representing, say, the Si(001) surface] at two different simulation times (time and length units are arbitrary). Similarly, insets of Figs. 1(c) and 1(d) correspond to the same simulations for a surface with a 10% higher SR ($\mathrm{SR}_{111}=1.1S_0$), thus representing the Si(111) orientation. The simulations reproduce in both cases the experimental coarsening and occurrence of a long-wavelength corrugation. In order to quantify the pattern features, we have analyzed systematically the PSD functions corresponding to 1+1 rather than 2+1 dimensional simulations due to the improved statistics of the former, since this dimensional reduction does not alter qualitatively the pattern coarsening and ordering properties.[19] The inset of Fig. 3(c) clearly shows that the pattern wavelength saturates earlier for the surface with higher SR, but the lower SR case attains a higher fina value. In addition, Fig. 3(c) shows that the correlation length also saturates earlier for a higher SR surface. Note that, as in the experimental AFM data and due to similar statistical limitations as compared with GID, the asymptotic ξ values are similar for both SR conditions. Remarkably, both AFM and simulation results agree in estimating ordered domains to contain roughly three nanodots across (namely, $\xi \sim 3\lambda$). This agreement between simulations and experimental observations allows us to conclude that the experimental differences observed between the pattern evolution on Si(111) and Si(001) surfaces are due to their different SRs.

In summary, we have studied by AFM and GID the temporal evolution of λ and ξ in IBS short-range hexagonal nanodot patterns on Si(001) and Si(111) surfaces. Due to its nonlocal character, GID is more reliable for quantificatio purposes than AFM. We have seen that the surface orientation does not determine the pattern formation qualitatively. However, our experimental and theoretical results show that through the dependence of the SR with the surface orientation, the latter becomes relevant to improve the degree of order of the pattern. For, e.g., technological purposes, it is worth noting that smaller SR allows for the increase in the fina size of ordered domains. The satisfactory comparison between the experimental results and numerical simulations highlights the physical relevance of relaxation mechanisms such as local redeposition and surface viscous flo .

This work has been supported by grants BFM2003-07749-C05-01, BFM2003-07749-C05-02, and BFM2003-07749-C05-05 from the Spanish Ministerio de Educación y Ciencia (MEC). Two of the authors (R.G. and J.M.-G.) acknowledge financia support from MEC through the "*Ramón y Cajal*" and FPU programs, respectively.

[1] *Springer Handbook of Nanotechnology*, edited by B. Bhushan (Springer, Berlin, 2004), p. 198.
[2] U. Valbusa, C. Boragno, and F. Buatier de Mongeot, J. Phys.: Condens. Matter **14**, 8153 (2002).
[3] M. Navez, C. Sella, and D. Chaperot, Acad. Sci., Paris, C. R. **254**, 240 (1962).
[4] S. Facsko, T. Dekorsy, C. Koerdt, C. Trappe, H. Kurz, A. Vogt, and H. L. Hartnagel, Science **285**, 1551 (1999).
[5] R. M. Bradley and J. M. E. Harper, J. Vac. Sci. Technol. A **6**, 2390 (1988).
[6] R. Gago, L. Vázquez, R. Cuerno, M. Varela, C. Ballesteros, and J. M. Albella, Appl. Phys. Lett. **78**, 3316 (2001).
[7] B. Ziberi, F. Frost, Th. Höche, and B. Rauschenbach, Phys. Rev. B **72**, 235310 (2005).
[8] T. H. Metzger, I. Kegel, R. Paniago, and J. Peisl, J. Phys. D **32**, A202 (1999).
[9] S. Facsko, T. Bobek, H. Kurz, T. Dekorsy, S. Krysta, and R. Cremer, Appl. Phys. Lett. **80**, 130 (2002).
[10] S. Habenicht and K. P. Lieb, Phys. Rev. B **65**, 115327 (2002).
[11] T. Bobek, S. Facsko, H. Kurz, T. Dekorsy, M. Xu, and C. Teichert, Phys. Rev. B **68**, 85324 (2003).
[12] M. Xu and C. Teichert, J. Appl. Phys. **96**, 2244 (2004).
[13] S. K. Tan and A. T. S. Wee, J. Vac. Sci. Technol. B **24**, 1444 (2006).
[14] O. Plantevin, R. Gago, L. Vázquez, and T. H. Metzger (unpublished).
[15] R. Cuerno and A.-L. Barabási, Phys. Rev. Lett. **74**, 4746 (1995); M. Makeev, R. Cuerno, and A.-L. Barabási, Nucl. Instrum. Methods Phys. Res. B **197**, 185 (2002).
[16] B. Kahng, H. Jeong, and A.-L. Barabási, Appl. Phys. Lett. **78**, 805 (2001).
[17] S. Facsko, T. Bobek, A. Stahl, H. Kurz, and T. Dekorsy, Phys. Rev. B **69**, 153412 (2004); S. Vogel and S. J. Linz, *ibid.* **72**, 35416 (2005).
[18] M. Castro, R. Cuerno, L. Vázquez, and R. Gago, Phys. Rev. Lett. **94**, 16102 (2005); J. Muñoz-García, M. Castro, and R. Cuerno, *ibid.* **96**, 86101 (2006).
[19] J. Muñoz-García, R. Cuerno, and M. Castro, Phys. Rev. E (to be published).